Live-cell single particle imaging reveals the role of RNA polymerase II in histone H2A.Z eviction

Anand Ranjan[1], Vu Q. Nguyen[1], Sheng Liu[1], Jan Wisniewski[2,3], Jee Min Kim[1], Xiaona Tang[1], Gaku Mizuguchi[1], Ejlal Elalaoui[1], Timothy J. Nickels[1], Vivian Jou[1], Brian P. English[3], Qinsi Zheng[3], Ed Luk[4], Luke D. Lavis[3], Timothee Lionnet[5], Carl Wu[1, 6, *]

[1]Department of Biology, Johns Hopkins University, Baltimore, MD 21218, USA

[2]Janelia Research Campus, Howard Hughes Medical Institute, Ashburn, VA 20147, USA

[3] Current address: Experimental Immunology Branch, National Cancer Institute, Bethesda, MD 20892, USA

[4]Department of Biochemistry and Cell Biology, Stony Brook University, Stony Brook, NY 11794, USA

[5]Institute of Systems Genetics, Langone Medical Center, New York University, New York, NY 10016, USA

[6]Department of Molecular Biology and Genetics, Johns Hopkins School of Medicine, Baltimore, MD 21287, USA

*Correspondence: wuc@jhu.edu (C.W.)

Abstract

The H2A.Z histone variant, a genome-wide hallmark of permissive chromatin, is enriched near transcription start sites in all eukaryotes. H2A.Z is deposited by the SWR1 chromatin remodeler and evicted by unclear mechanisms. We tracked H2A.Z in living yeast at single-molecule resolution, and found that H2A.Z eviction is dependent on RNA Polymerase II (Pol II) and the Kin28/Cdk7 kinase, which phosphorylates Serine 5 of heptapeptide repeats on the carboxy-terminal domain of the largest Pol II subunit Rpb1. These findings link H2A.Z eviction to transcription initiation, promoter escape and early elongation activities of Pol II. Because passage of Pol II through +1 nucleosomes genome-wide would obligate H2A.Z turnover, we propose that global transcription of noncoding RNAs prior to premature termination, in addition to transcription of mRNAs, are responsible for eviction of H2A.Z. Such usage of yeast Pol II suggests a general mechanism coupling eukaryotic transcription to erasure of the H2A.Z epigenetic signal.

Introduction

The H2A.Z variant of canonical histone H2A serves as a key chromatin constituent of the epigenome, providing a unique nucleosome architecture and molecular signature for eukaryotic gene transcription and other chromosome activities (Weber and Henikoff, 2014). H2A.Z is enriched at most promoters and enhancers genome-wide, and plays a role in establishing a permissive chromatin state for regulated transcription (Weber and Henikoff, 2014). H2A.Z is incorporated in nucleosomes flanking DNase hypersensitive, nucleosome-depleted regions (NDRs), especially at the so-called '+1 nucleosome' overlapping with or immediately downstream of the transcription start site (TSS) (Albert et al., 2007; Weber and Henikoff, 2014). The deposition of H2A.Z in budding yeast is catalyzed by the conserved SWR1 chromatin remodeling complex in an ATP-dependent reaction involving exchange of nucleosomal H2A-H2B for H2A.Z-H2B dimers (Mizuguchi et al., 2004).

Genome-wide studies have shown that compared to nucleosomes in the gene body, the +1 nucleosome undergoes higher turnover, which is not correlated with the level of mRNA transcription by Pol II (Dion et al., 2007; Grimaldi et al., 2014; Rufiange et al., 2007). Thus, the disruptive passage of Pol II through +1 nucleosomes during infrequent mRNA transcription is unlikely to account for H2A.Z eviction on a global scale. Biochemical studies have suggested that yeast H2A.Z eviction could be due to chromatin remodeling in reverse mediated by SWR1 itself (Watanabe et al., 2013) or the related INO80 remodeler (Papamichos-Chronakis et al., 2011), but other studies found no supporting evidence (Wang et al., 2016). Alternatively, genome-wide assembly

of the transcription pre-initiation complex (PIC) has been proposed to evict H2A.Z, but the key event in this multistep process remains elusive (Tramantano et al., 2016). To determine the dominant mechanism of H2A.Z turnover after incorporation, we took an independent approach using single-particle tracking that directly measures the levels of chromatin-free and bound H2A.Z in the physiological environment of living yeast cells, in wild type and conditional mutants for histone eviction.

Single-particle tracking (SPT) of fluorescently tagged proteins in live cells has emerged as a robust imaging technique to determine kinetic behaviors of protein factors (Elf and Barkefors, 2018; Liu and Tjian, 2018). For chromatin-interacting proteins, SPT is complementary to genome-wide chromatin immunoprecipitation-DNA sequencing technologies (ChIP-seq) without the general caveats of chemical fixation and chromatin manipulations. SPT directly measures the fast-diffusing, chromatin-free population as well as the quasi-immobile, chromatin-bound fraction tracking with macroscopic chromosome movements (Liu and Tjian, 2018; Taddei and Gasser, 2012).

Results

We fused the self-labeling HaloTag to H2A.Z, H2B, and Swr1 (the catalytic subunit of the SWR1 complex) for sole source expression under native promoter control and validated the function of these fusion constructs (Fig. S1.1A). Yeast cultures were fluorescently labeled to saturation with Janelia Fluor 646 (Grimm et al., 2015) (Fig. S1.1B, C), and movies of single molecules were recorded at high temporal resolution (10 ms exposure) in live cells (Rust et al., 2006) (Movies S1-6). Single molecule

trajectories (n>1000 and ≥6 frames for each trajectory) were obtained from over 50 yeast cells for each strain. The data is presented as histograms of particle frequency over the diffusion coefficient (log D) extracted from mean squared displacements (MSD) (Fig. 1 A-D, and methods). For a more robust quantitation of diffusive populations, we also applied a kinetic modeling approach ('Spot-On') based on single particle displacements (Hansen et al., 2018) (Fig. 1E, F). We performed Spot-On analysis on single-molecule trajectories (≥3 frames), cite Spot-On values for chromatin-bound and chromatin-free fractions in the text, and provide results from both Spot-On and MSD analyses in all figures.

The SPT profiles for H2A.Z and H2B were best fitted by a simple model comprised of two diffusive populations—a major, slow-diffusing chromatin-bound fraction (H2A.Z: 82%, H2B: 76%, average D: 0.03 $\mu m^2 s^{-1}$), and a minor, fast-diffusing chromatin-free fraction (H2A.Z: 1.18 $\mu m^2 s^{-1}$, H2B: 1.29 $\mu m^2 s^{-1}$) (Fig. 1E, F & Fig. S1.2A, B, E). Additional minor populations of H2A.Z and H2B with distinct diffusive values are not excluded. The fraction of chromatin-bound H2A.Z was consistent with a previous estimate by *in vivo* cross-linking (Mohan et al., 2018), and the D value of bound yeast H2B was also consistent with that of mammalian H2B (0.02 $\mu m^2 s^{-1}$) in a previous report (Hansen et al., 2018). The 'free' H2A.Z fraction represents soluble H2A.Z-H2B dimers biochemically associated with histone chaperones, in addition to a minor population in complex with the ~1 MDa SWR1 complex (Luk et al., 2007). We observed similar frequencies of chromatin-bound and free H2A.Z in cells growing synchronously after release from G1 arrest into S phase (Fig. S1.3).

In contrast to the steady-state behaviors of the histones, the SWR1 complex (Swr1-Halo subunit) showed more chromatin-free diffusion. In addition, deletion of Swc2, a key subunit involved in the recruitment of SWR1 to gene promoters (Ranjan et al., 2013), substantially reduced the chromatin-bound fraction from 47% to 21% (Fig. 1C, D, F). (Our imaging regime captures both stable and transiently bound SWR1 in the slow-diffusing population; the remaining 21% of slow molecules for the *swc2*Δ mutant may be largely attributed to transient binding). With these validations, we proceeded to investigate regulators of H2A.Z dynamics, based on the fractional changes in chromatin-bound and free H2A.Z. Notably, while the aforementioned labeling of HaloTag was adequately conducted with the JF646 dye, a superior flurophore JF552 became available in the course of this work, prompting its use in subsequent experiments for improved signal to noise (Zheng et al., 2019). (Fig. S1.1F).

The steady-state chromatin occupancy for H2A.Z is a function of competing deposition and eviction pathways. To highlight H2A.Z eviction in live cells, we blocked the H2A.Z incorporation pathway at gene promoters by conditional 'anchor-away' (AA) depletion of the Swc5 subunit, which is not required for Swr1 recruitment (Fig. S2.1), but essential for SWR1 activity (Haruki et al., 2008; Sun and Luk, 2017; Tramantano et al., 2016). In the AA system, rapamycin mediates heterodimerization of FRB and FKBP12 moieties fused to Swc5 and the ribosomal protein RPL13A, respectively (i.e. Swc5-FRB and RPL13A-FKBP12), thus depleting Swc5 from the nucleus along with pre-ribosomal subunit export (Haruki et al., 2008). Upon Swc5 AA, we found the expected decrease of chromatin-bound H2A.Z from 79% to 49% (Fig. 2A-C), consistent with ChIP-seq results

showing genome-wide reduction of H2A.Z at +1 nucleosomes under similar conditions (Tramantano et al., 2016). The remaining chromatin-bound H2A.Z may be due to histone chaperone-mediated H2A.Z deposition in nucleosomes over the entire genome, as suggested by in vivo cross-linking studies (Mohan et al., 2018). Our live-cell findings thus confirm the SWR1 requirement for H2A.Z deposition.

To identify H2A.Z eviction factors, we tested candidates that could inhibit the loss of chromatin-bound H2A.Z when both deposition and eviction factors were co-depleted in a double AA experiment. As the transcription PIC is constitutively enriched at the majority of NDRs (Rhee and Pugh, 2012) and has been causally linked to H2A.Z eviction (Tramantano et al., 2016), we first imaged the distribution of H2A.Z after nuclear depletion of both Swc5 and the Rpb1 catalytic subunit of Pol II. When Swc5 and Rpb1 are co-depleted by double AA, the chromatin-bound H2A.Z fraction increased (66%) relative to Swc5 AA alone (49%) (compare Fig. 3A to 2C and 3C to 2D). Fluorescence microscopy confirmed relocation of Swc5 to the cytoplasm in double AA cells, excluding inefficient nuclear depletion as a caveat (Fig. S3.1C, D). These results indicate that Pol II indeed plays a major role in H2A.Z eviction. (Single AA of Rpb1 in rapamycin-treated cells showed a marginal increase from 84% to 87% of the bulk chromatin-bound H2A.Z over the untreated control (Fig. S3.2A-C)).

To examine the role of the INO80 remodeler in H2A.Z eviction, we analyzed the H2A.Z distribution for Swc5 and Ino80 co-depletion by double AA and found no rise in bound H2A.Z compared to the single AA of Swc5 (compare Fig. 3B to 2C and 3C to 2D). (We

observed no change in chromatin-bound H2A.Z for single AA of Ino80 (Fig S3.2D-F)). Taken together, we conclude that Pol II, but not the INO80 remodeler, has a major role in H2A.Z eviction. Minor contributions by other factors such as the ANP32E histone chaperone found in mammalian cells are not excluded (Mao et al., 2014; Obri et al., 2014).

Transcription by Pol II is a complex process involving PIC assembly, Pol II initiation, promoter escape, productive elongation and termination (Jonkers and Lis, 2015; Sainsbury et al., 2015). Given that site-specific phosphorylation of the Rpb1 subunit of Pol II regulates the progression of transcription, targeted depletion of transcriptional kinases provides an opportunity to identify the step involved in H2A.Z eviction. A key post-initiation step involves Serine 5 phosphorylation (Ser5-P) of heptapeptide repeats on the C-terminal domain (CTD) of Pol II (Rpb1) (Corden, 2013; Harlen and Churchman, 2017). Ser5-P is catalyzed by the yeast Kin28/Cdk7 kinase, a component of the kinase module (Kin28-Ccl1-Tfb3) of TFIIH, and is linked to capping of nascent RNA, Pol II release from the Mediator complex, promoter escape and early elongation. Recently, the Bur1/Cdk9 kinase was shown to phosphorylate the Rpb1 linker just upstream of CTD, at residues Thr 1471 and Ser 1493 (Chun et al., 2019), facilitating Pol II transition from early elongation to productive elongation**.** Furthermore, the Ctk1/Cdk12 kinase mediates Ser2 phosphorylation of the CTD associated with productive elongation through protein-coding regions (Corden, 2013; Harlen and Churchman, 2017; Wong et al., 2014). To investigate which phosphorylated state of Pol II is linked to H2A.Z eviction, we examined H2A.Z distributions in double AA cells conditionally deficient for

Swc5 in combination with each of the three CTD kinases. Only Kin28 is required for H2A.Z eviction, as indicated by 65% chromatin-bound H2A.Z in the Kin28 and Swc5 double AA relative to 49% in the single AA of Swc5 (compare Fig. 4B to 2C and 4F to 2D). Consistent with its role in H2A.Z eviction, depletion of Kin28 alone showed a marginal 4% increase in chromatin-bound H2A.Z (from 78% to 82%, Fig. S4.1A, 4.1B). In contrast, double AA of Swc5 and the Bur1 kinase did not inhibit loss of chromatin-bound H2A.Z, nor did double AA of Swc5 and the Ctk1 kinase (Fig. 4C, 4D, 4F).

In the wake of Pol II initiation, nascent RNA is co-transcriptionally capped by the sequential activity of three enzymes—Cet1, Ceg1 and Abd1—and is completed when RNA reaches ~100 nt (Lidschreiber et al., 2013). Capping of the 5' end of nascent RNA is initiated by the Cet1-Ceg1 complex, which recognizes the 5' triphosphate on the RNA and Ser5-P on the Pol II CTD (Martinez-Rucobo et al., 2015). To examine whether RNA capping or associated activities are required for H2A.Z eviction, we performed double AA of Swc5 and Cet1, and found no increase in chromatin-bound H2A.Z compared to single AA of Swc5 (compare Fig. 4E, to 2C, and 4F to 2D). Thus, H2A.Z eviction is not dependent on RNA capping. Likewise, we found no increase of chromatin-bound H2A.Z upon double AA of Swc5 and Rrp6, the 3'-5' exonuclease responsible for degradation of noncoding RNA (Fig. S4.1E, F). Taken together, we conclude that an early stage of transcription elongation closely linked to Pol II CTD Ser5 phosphorylation by Kin28 is required for robust eviction of chromatin-bound H2A.Z.

Discussion

Transcription of most yeast genes is infrequent and nucleosome turnover along gene bodies is low, but the +1 nucleosome constitutively turns over at a 3-fold higher rate (Dion et al., 2007; Grimaldi et al., 2014; Yen et al., 2013). Similarly, H2A.Z is constitutively displaced from +1 nucleosomes for both active and rarely transcribed genes, on a timescale of <15 min (Tramantano et al., 2016). The live-cell SPT approach reveals that Pol II rather than the INO80 sub-family of remodelers plays a key role in H2A.Z eviction. Furthermore, the dependence on Kin28/Cdk7 kinase for robust H2A.Z displacement suggests that PIC assembly per se, i.e. the recruitment of general transcription factors and Pol II to promoter, is not sufficient for H2A.Z eviction but Kin28-dependent phosphorylation of Ser5 of the CTD heptapeptide repeats is important (Fig. 5, box). A role for Kin28 in Ssl2-facilitated TSS scanning by Pol II is not excluded for H2A.Z eviction, although it has been shown that depletion of Kin28 by AA does not alter TSS usage (Murakami et al., 2015).

Inhibition of H2A.Z eviction upon depletion of Kin28/Cdk7 kinase, but not Bur1/Cdk9 or Ctk1/Cdk12 kinases narrows the relevant state of Pol II to early elongation after promoter escape, but not to productive elongation. (We note that the PIC remains largely intact upon Kin28/Cdk7 depletion, as shown by accumulation of TFIID, Mediator and Pol II at gene promoters (Knoll et al., 2019) (Wong et al., 2014)).The exclusive dependence on Kin28/Cdk7 is further underscored by no reduction of H2A.Z eviction on depletion of Cet1, the 5’ RNA capping enzyme, or depletion of Rrp6, the 3’-5’ exonuclease for noncoding RNA degradation. Thus, H2A.Z eviction is independent of

RNA modifiying and metabolizing activities just downstream of CTD Ser5 phosphorylation.

Transcriptional elongation by Pol II is known to cause displacement of nucleosomal histones in biochemical assays (Lorch et al., 1987), providing a mechanism for H2A.Z turnover at the +1 nucleosome in the process of transcription through protein-coding regions. We propose a similar mechanism for genes that do not engage in productive transcription of mRNA, but exhibit genome-wide, constitutive transcription of noncoding RNAs which are prematurely terminated by the Nrd1-Nab3-Sen1 pathway in budding yeast (Schaughency et al., 2014). The early elongation activity of Pol II would dislodge H2A.Z-H2B dimers from the histone octamer of the +1 nucleosome. Displacement of the more stably bound H3-H4 tetramer likely requires assistance from histone chaperones and/or other remodelers (Fig 5).

After displacement of core histones, reassembly of a canonical nucleosome on gapped chromatin should occur, mediated by the mass action of the predominating H2A-H2B histone pool and histone chaperones, nucleosome positions being reset by chromatin remodelers such as ISWI, RSC, and INO80 (Lai and Pugh, 2017) (Fig.5)**.** Maintenance of a NDR of sufficient length (>60 bp DNA) by remodelers and subsequent histone acetylation recruits SWR1 to canonical +1 nucleosomes, the essential substrate for SWR1 (Ranjan et al., 2013). Stimulation of the catalytic Swr1 ATPase by nucleosome and H2A.Z-H2B dimer substrates then triggers histone dimer exchange (Luk et al., 2010; Ranjan et al., 2013), completing the cycle of H2A.Z/H2A replacement (Fig. 5).

We envision that H2A.Z eviction is coupled to transcription not only from protein-coding genes transcribed by Pol II but also ribosomal, 5S and tRNA genes transcribed by Pol I and Pol III. Because H2A.Z eviction is not correlated with mRNA transcription by Pol II (Tramantano et al., 2016), the constitutive global transcription of noncoding RNA by Pol II is additionally coupled to H2A.Z eviction. There is substantial evidence for low-level, heterogenous transcripts of several hundred nucleotides, initiating from multiple start-sites within yeast NDRs (Pelechano et al., 2013). For budding yeast, these noncoding RNA transcripts evidently result from Pol II initiation without substantial pausing (Booth et al., 2016). At metazoan promoters, turnover of H2A.Z enriched in +1 nucleosomes may be similarly coupled to transcription in the process of Pol II pausing and release (Tome et al., 2018). Likewise at metazoan enhancers, infrequent Pol II transcription of eRNAs (Tippens et al., 2018) could be responsible for eviction of H2A.Z, representing erasure of a permissive histone variant mark on the epigenome. Much remains to be learned about the functional significance of this process and its relationship to productive mRNA transcription, presenting an outstanding problem for future studies of chromatin dynamics in eukaryotic gene regulation.

Acknowledgements

This work is dedicated to the memory of Maxime Dahan, former project leader of the HHMI-Janelia Transcription Imaging Consortium. We thank Anita Corbett for reagents, Zhe Liu, Brian Mehl, and Herve Rouault for discussions, Felix Wu for image processing, Anders Hansen, Maxime Woringer, and Xavier Darzacq for consultation on the Spot-On program, Prashant Mishra and Munira Basrai for assistance with FACS analysis, and James Brandt and Yumi Kim for deconvolution microscopy. The study was supported by HHMI-Janelia Transcription Imaging Consortium funding to C.W., T.L., and L.L, the Damon Runyon Cancer Research Foundation (V.N.), the Johns Hopkins Bloomberg Distinguished Professorship (C.W.), a grant to E.L. from the National Institutes of Health (GM104111), a grant to T.L. from National Institutes of Health (GM127538), and a grant to C.W. from the National Institutes of Health (GM125831).

Figure Legends

Figure 1. Diffusive behaviors of protein fusions to HaloTag (Halo) reveal chromatin-bound and free populations in live yeast. (A, B) Normalized histograms and two-component Gaussian fits for H2A.Z-Halo (A) and Halo-H2B (B) show the log diffusion coefficient distributions. The Gaussian fit for HaloTag is shown for reference ("Halo only" in A). (C, D) Normalized histograms and two-component Gaussian fits for Swr1-Halo in WT cells (C) and the *swc2Δ* mutant (D). Solid line: sum of two-component fit; dashed line: individual component. Percent value of the slow component along with Bootstrap resampling errors and the number of trajectories (n) are indicated. (E) Cumulative distribution functions (CDF) of 10 ms displacements. (F) Spot-On results with fitting errors showing fractions of chromatin-bound molecules derived from modeling CDFs over 10-50 ms intervals. All molecules tracked with JF646 dye except Halo only, which was imaged with JF552.

Figure S1.1. Cell growth, labeling and SPT analysis of Halo-tagged proteins (A) Growth of strains bearing *SWR1*, H2A.Z (*HTZ1)* and H2B *(HTB1)* fusions to HaloTag. Saturated cultures at optical density 1.0 were spotted (1:5 serial dilutions) on CSM plates with or without 1% formamide or 150 mM HU (hydroxyurea) and incubated for 2-3 days at the indicated temperatures. WT and mutant strains *htz1Δ* and *swr1Δ* are shown for comparison. (B) Cells expressing H2A.Z-Halo and Swr1-Halo were stained with JF646 and the cell lysate was resolved on SDS-PAGE. Fluorescent scan of duplicate lanes show specific labeling of Halo-tagged H2A.Z and Swr1 proteins. (C) SDS-PAGE shows 10 nM JF646 saturates H2A.Z-Halo in yeast cells in a routine 2 hr

staining period. (D) Normalized histogram and two-component Gaussian fit for HaloTag (fused to NLS). The slow fraction is 5%. (E) Top: Profile of H2A.Z-Halo diffusivity in biological replicate, same condition as Fig. 1A experiment. (F) Profile of H2A.Z-Halo diffusivity in cells stained with JF552. All molecules tracked with JF552 dye except (E), which was tracked with JF552.

Figure S1.2. Spot-On kinetic modeling analysis. (A) Histogram of displacements over time intervals of 10, 20, 30, 40 and 50 ms (dt 1-5) for H2A.Z. First four displacements were included for each track. Kinetic fitting shown as dashed line and measured displacements in color. Data was generated using the Spot-On web-interface (https://SpotOn.berkeley.edu). (B) Spot-On analysis of H2B. (C,D) Spot-On analysis of Swr1 in WT and *swc2Δ* cells. (E) Comparison of diffusive parameters for H2A.Z, H2B, Swr1 and Swr1 in the *swc2Δ* strain, extracted from MSD-based and Spot-On analytic platforms. Bootstrap resampling errors shown for MSD and fitting errors shown for Spot-On. All molecules tracked with JF646 dye.

Figure S1.3. H2A.Z-Halo distribution in cell division cycle. (A) FACS analysis shows DNA content of the synchronized cell population upon time of release from α-factor arrest, from 0' – 120.' (B,C) Normalized histogram and two-component Gaussian fit for H2A.Z-Halo in cells synchronized in pre-S phase, and in S phase. (D) Spot-On results shows both Pre-S and S phase cells have 84 % chromatin bound H2A.Z. All molecules tracked with JF646 dye.

Figure 2. H2A.Z chromatin binding is substantially reduced upon abrogation of the deposition pathway by SWR1 inactivation. (A) Time course of H2A.Z-Halo labeling, rapamycin treatment and image acquisition in Swc5-AA cells. Rapamycin treatment for an hour before SPT, and imaging perfomed in continued presence of rapamycin. (B, C) Normalized histograms and two-component Gaussian fits for H2A.Z-Halo imaged in the Swc5-AA cells. Imaging data were acquired in absence of rapamycin (B) or presence of rapamycin (C). Spot-On results show that Swc5 depletion causes a reduction in chromatin-bound H2A.Z. (E) Overlay of tracks, color-coded according to log diffusion coefficients, obtained from representative nuclei. Number of tracks (n) is indicated for each nucleus. All molecules tracked with JF552 dye.

Figure S2.1. Swc5 is required post-recruitment for SWR1 activity. (A,B) Normalized histograms and two-component Gaussian fits for Swr1-Halo imaged in Swc5-AA cells in the absence (A) or presence (B) of rapamycin. (C) Spot-On analysis of the same imaging data. Anchor away of Swc5 did not reduce the fraction of chromatin-bound Swr1, which is consistent with ChIP-PCR results showing Swr1 binds to gene promoters in absence of swc5 (Morillo-Huesca et al., 2010), and *in vitro* data showing efficient nucleosome binding by the purified SWR1(swc5Δ) complex (Ranjan et al., 2013). All molecules tracked with JF646 dye.

Figure 3. RNA polymerase II is critical for H2A.Z eviction. (A) Normalized histograms and two-component Gaussian fits for H2A.Z-Halo imaged in cells co-depleted for Rpb1 and Swc5. (B) H2A.Z-Halo distributions in cells co-depleted for Ino80

and Swc5. (C) Spot-On results showing co-depletion of Rpb1 along with Swc5 inhibits H2A.Z eviction. All molecules tracked with JF552 dye.

Figure S3.1. Efficient nuclear depletion of Swc5 in double anchor-away (*SWC5-FRB; RPB1-FRB*) strain. (A, B) Deconvolution fluorescence microscopy shows nuclear depletion of Swc5-AA in rapamycin-treated, single anchor-away cells, and in Swc5-AA; Rpb1-AA double anchor-away cells. Images of JF646-labeled H2A.Z-Halo locate nuclei. Z-axis steps of 200 μm were captured on a DeltaVision fluorescence microscope and deconvoluted ten-stacks were projected.

Figure S3.2. H2A.Z diffusion histograms in cells for single AA of Rpb1 and Ino80. (A, B) H2A.Z-Halo distributions in Rpb1-AA strain without (A) and with (B) depletion of Rpb1. (C) Spot-On results for chromatin bound H2A.Z upon Rpb1 depletion. Single AA of Rpb1 causes only a slight increase in chromatin-bound H2A.Z, which is likely due to concomitant inhibition of SWR1's biochemical activity at reduced concentration of free H2A.Z-H2B dimer (Wang et al., 2016). (D, E) H2A.Z distributions in single anchor-away of Ino80. (F) Spot-On results show Ino80 depletion has no effect on level of chromatin-bound H2A.Z. All molecules tracked with JF552 dye.

Figure 4. Kin28 phosphorylation of RNA polymerase II CTD is critical for H2A.Z eviction. (A) Schematic representation shows the three Pol II kinases Kin28, Bur1 and Ctk1 recruited at initiation, early-elongation and elongation phases respectively of Pol II and corresponding phosphorylation of indicated Rpb1 CTD sites. Set1 is the first of the

three RNA capping enzymes; it removes γ-phosphate from the RNA 5' end to generate 5' diphosphate. (B, C, D, E) Normalized histograms and two-component Gaussian fits for H2A.Z-Halo imaged in cells co-depleted for Swc5 along with Kin28 (B), Bur1 (C), Ctk1 (D) and Cet1 (E). (F) Spot-On results show Kin28 is required to evict H2A.Z. All molecules tracked with JF552 dye.

Figure S4.1. H2A.Z diffusion histograms in cells after single depletion of Kin28. (A, B) H2A.Z-Halo distributions in Kin28-AA strain without (A)and with (B) depletion of Kin28. (C) Spot-On results for chromatin bound H2A.Z upon Kin28 depletion. (D) Reproduction of Gaussian fits for H2A.Z-Halo distributions in rapamycin-treated Swc5-AA cells (from Fig. 2C). (E) H2A.Z-Halo distributions in cells co-depleted for Swc5 and Rrp6. (F) Spot-On results for chromatin-bound H2A.Z upon double depletion of Swc5 and Rrp6. All molecules tracked with JF552 dye.

Figure 5. Cycle of H2A.Z eviction and deposition. RNA polymerase II assembled genome-wide in the PIC and Rpb1 CTD Ser5 phosphorylated by Kin28 constitutively transcribes short noncoding RNAs (with m7G cap) and evicts H2A.Z-H2B dimers from the +1 nucleosome prior to termination. H2A.Z eviction should also occur in the course of mRNA transcription. Additional factors may be necessary for displacement of H3-H4 tetramer. The directional arrow indicates the annotated transcription start site. The gap is filled by histone chaperone-mediated deposition of canonical histones to reform an H2A-containing +1 nucleosome, which is positioned by chromatin remodelers and sequence-specific transcription factors, maintaining the NDR. This recruits SWR1 which

is activated upon recognition of H2A-nucleosome and H2A.Z-H2B dimer substrates to activate one or two rounds of H2A.Z deposition. See text for discussion.

List of Supplementary Movies and Table

Movie S1: H2A.Z-Halo imaged in wild type cells. Single molecules from four nuclei are observed.

Movie S2: H2A.Z-Halo imaged after anchor-away of Swc5. Single molecules from six nuclei are observed.

Movie S3: H2A.Z-Halo imaged in Swc5-FRB cells in absence of rapamycin. Single molecules from four nuclei are observed.

Movie S4: Swr1-Halo imaged in wild type cells. Single molecules from three nuclei are observed.

Movie S5: Swr1-Halo imaged in *swc2*Δ cells. Single molecules from three nuclei are observed.

Movie S6: Free-Halo tag molecule imaged in nuclei. Single molecules from five nuclei are observed.

Supplementary file 1: List of strains used in this study

Supplementary file 2: List of results from MSD and Spot-On analysis

Materials and Methods

Yeast strains and plasmids

The plasmid for HaloTag (Halo) fusions was generated by cloning HaloTag (Promega) in the pBluescript SK (-) vector followed by insertion of a KanMx cassette (Kanamycin) or NatMx cassette (Nourseothricin), following standard procedures (Gelbart et al., 2001). PCR amplification and standard yeast transformation methods were used for tagging the protein of interest at the C-terminus, with a serine-glycine $(SG_4)_2$ linker to HaloTag.

For Halo-H2B, plasmid HTA1-SNAP-HTB1 (pEL458, gift from Ed Luk) was modified to replace the SNAP coding sequence with HaloTag, with a four amino acid GA_3 linker between HaloTag and the N-terminus of H2B. The plasmid expressing Halo-H2B was introduced in the FY406 strain (gift from Fred Winston) by the plasmid shuffle procedure (Hirschhorn et al., 1995). The endogenous H2B promoter drives expression of Halo-H2B as the sole gene copy in cells.

Free HaloTag was fused at the N-terminus to a bipartite SV40 NLS (KRTADGSEFESPKKKRKV, where two clusters of basic residues are underlined) (Hodel et al., 2006) and expressed from the pRS416 vector. Plasmid pAC1056 expressing BPSV40 NLS-GFP (gift from Anita Corbett) was modified for free Halo expression.

Strains and plasmids used for anchor-away studies were obtained from Euroscarf. The transporter gene PDR5 was deleted in all strains for retention of HTL-dye conjugate in live yeast cells. Strain genotypes are listed in Table 1.

Flow cytometry analysis

Cells were fixed by adding two volumes of 100 % ethanol and stored for one hour at 4˚C. Cells were washed with 50 mM Tris-HCl (pH 7.5) buffer and digested with RNase (1 mg/ml) and RNase A (0.2 mg/ml) overnight at 37˚C on a rotator. Proteins were digested with Proteinase K (1 µg/µl) at 50˚C for 30 minutes. Cells were stained with 2 µM SYTOX (Tris buffer) at 4˚C for 4 hours and sonicated on Diagenode Biorupter 300 for 10 sec at high setting. Cells were scanned on LSR II FACS instrument.

Cell culture and labeling

Cells were grown and imaged in CSM media (Complete Supplement Mixture) supplemented with 40 mg/L adenine hemisulfate. The JF646-HaloTag ligand was synthesized as previously described (Grimm et al., 2015). The new JF552 dye has a higher signal to noise ratio and is more photostable than JF646. The JF552 dye is a modification of JF549, with similar brightness, but enhanced cell permeability that allows its use for SPT in yeast (Zheng et al., 2019). For *in vivo* labeling, early log phase cells ($O.D_{600}$ 0.2) were labeled with JF-HaloTag ligand (10 nM for JF646 and 20 nM for JF552) for two hours at 30 degrees in suspension culture. Cells were washed four times with CSM to remove free dye.

Prior to use, 0.17 mm coverslips (Ø 25 mm, Electron Microscopy Services) were flamed to remove punctuated surface auto-fluorescence and to suppress dye binding, and coated with Concanvalin A (2 mg/ml) for 30 min at room temperature, and air-dried for one hour. Coverslips were assembled in a Ø 35 mm Attofluor chamber (Invitrogen). A 1 ml cell suspension was immobilized for 10 minutes and live cells were imaged in CSM media at room temperature. For anchor away experiments, rapamycin (1 µg/ml) was added one hour prior to imaging, and cells were imaged in the presence of rapamycin.

Cell cycle synchronization

Cells were synchronized in G1 by adding α factor for 2 hours (3 µg/ml at 0 min and additional 2 and 1 µg/ml at 60 and 90 minute respectively). High autofluoresence did not allow SMT in presence of α factor, which was removed by replacing culture medium. Cells released from G1 at room temperature took 40 minutes to enter S phase. Both for Pre-S and S phase SMT, cells were stained and synchronized in suspension culture and immobilized right before SMT.

Wide-field single molecule Imaging with epi-Illumination microscope

Single-molecule imaging was conducted on a Zeiss Observer Z1 microscope with a Zeiss Plan-Apochromat 150X/1.35 glycerin-immersion objective. Cells of interest were identified under infrared illumination (750nm, 10nm FWHM) using a near IR-CCD camera (IDS UI-3370CP-NIR-GL) and Semrock 743nm/25nm FWHM filter. A 555nm (Crystalaser) or 637nm (Vortran) laser was used for dye excitation, typically at 100mW total power (TTL pulsed). All laser beams were spectrally filtered and combined using a

custom beam combiner (by J.W., details available upon request). A Semrock FF01-750/SP filter was included at the output to remove any residual near infrared emission from lasers. Combined laser beams were collimated into a 2m-long Qioptic fiber (kineFLEX-P-2-S-405.640-0.7-APC-P2) with output through a 12mm EFL reflective collimator (Thorlabs). The resulting Ø6mm Gaussian beam was introduced into the back port of the microscope. The following cubes were utilized in the microscope turret to direct excitation light towards the sample and filter fluorescence: 1) for JF646 - 648 beamsplitter and 676/29 nm filter, 2) for JF552 - 561 beamsplitter and 612/69 nm filter. Images were acquired with a Hamamatsu C9100-13 back-illuminated EM-CCD camera through additional FF01-750/SP and NF03-405/488/561/635E quad-notch filters. The camera was operated at -80°C with a typical EM gain of 1200 and directly controlled by laser emission via the TTL signal.

Image acquisition

Images were obtained using either 637-nm laser (JF646) or 555-nm laser (JF552), of excitation intensity ~1KW/cm^2 and for each field of view ~7000 frames were captured. Single molecules were tracked using DiaTrack Version 3.05 software, with the following settings; remove blur 0.1, remove dim 70-100, maximum jump 6 pixels. Single molecule images were collected after pre-bleach of initial intense fluorescence (glow). While imaging with JF646, a 405-nm laser excitation (1-10mW/cm^2, TTL pulses 2-5 ms per frame) was triggered to maintain single fluorophore detection density. Immobilized cells in CSM media were imaged over a 90-minute imaging session.

474 **Analysis of single-molecule images**

475 Movies with two dimensional single molecule data were analyzed by DiaTrack Version
476 3.05 (Vallotton and Olivier, 2013), which determines the precise position of single
477 molecules by Gaussian intensity fitting and assembles particle trajectories over multiple
478 frames. In Diatrack remove blur was set to 0.1, remove dim set at 70 and max jump set
479 at 5 pixels, where each pixel was 107 nm. Trajectory data exported from Diatrack was
480 further analyzed by a custom computational package 'Sojourner' (by S.L.). The package
481 is available on Github (https://rdrr.io/github/sheng-liu/sojourner/). The Mean Squared
482 Displacement (MSD) was calculated for all trajectories 6 frames or longer. Diffusion
483 coefficients for individual molecules were calculated by unconstrained linear fit ($R_2 > 0.8$)
484 of the MSD values computed for time lags ranging from 2 dt to 5 dt, where dt = 10 ms is
485 the time interval between frames, and slope of linear fit was divided by 4 (pre-factor for
486 2-dimensional brownian motion) (Qian et al., 1991). The histogram of log converted
487 diffusion coefficients was fitted with double gaussian function from the 'mixtools'
488 package (Benaglia et al., 2009) to estimate the fraction of chromatin-bound molecules
489 (mean range between 0.050 - 0.112 $\mu m^2 s^{-1}$). Standard error on the mean of each
490 gaussian fit parameter was estimated using a bootstrap resampling approach (Efron,
491 1979).
492
493 The Spot-On analysis was performed on trajectories three frames or longer using the
494 web-interface https://spoton.berkeley.edu/ (Hansen et al., 2018). The bound fractions
495 and diffusion coefficients were extracted from the CDF of observed displacements over
496 different time intervals. For Brownian motion in two dimensions, the probability that a

particle starting from origin will be found within a circle of radius r at time interval $\Delta\tau$ is given as follows.

$$P(r,\Delta\tau) = \frac{r}{2D\Delta\tau} e^{\frac{-r^2}{4D\Delta\tau}}$$

where D is diffusion coefficient. In Spot-On, the cumulative displacement histograms were fitted with a 2-state model.

$$p(r,\Delta\tau) = F_1 \frac{r}{2(D_1\Delta\tau+\sigma^2)} e^{\frac{-r^2}{4(D_1\Delta\tau+\square^2)}} + Z_{CORR}(\Delta\tau,\Delta Z,D_2)F_2 \frac{r}{2(D_1\Delta\tau+\sigma^2)} e^{\frac{-r^2}{4(D_1\Delta\tau+\sigma^2)}}$$

where F1 and F2 are bound and free fractions, σ is single molecule localization error, D1 and D2 are diffusion coefficients of bound and free fractions, and Z_{CORR} is correction factor for fast molecules moving out of axial detection range (Hansen et al. 2018). The axial detection range for JF646 on our setup is 650 nm. The following settings were used on the Spot-On web interface: bin width 0.01, number of time points 6, jumps to consider 4, use entire trajectories-No, Max jump (μm) 1.2. For model fitting the following parameters were selected: D_{bound} (μm^2/s) min 0.001 max 0.1, D_{free} (μm^2/s) min 0.15 max 5, F_{bound} min 0 max 1, Localization error (μm)- Fit from data-Yes min 0.01 max 0.1, dZ (μm) 0.65 for JF646 and dZ 0.6 for JF552, Use Z correction- Yes, Model Fit CDF, Iterations 3.

References

Albert, I., Mavrich, T.N., Tomsho, L.P., Qi, J., Zanton, S.J., Schuster, S.C., and Pugh, B.F. (2007). Translational and rotational settings of H2A.Z nucleosomes across the Saccharomyces cerevisiae genome. Nature *446*, 572-576.

Benaglia, T., Chauveau, D., Hunter, D.R., and Young, D.S. (2009). mixtools: An R Package for Analyzing Finite Mixture Models. J Stat Softw *32*, 1-29.

Booth, G.T., Wang, I.X., Cheung, V.G., and Lis, J.T. (2016). Divergence of a conserved elongation factor and transcription regulation in budding and fission yeast. Genome Res *26*, 799-811.

Chun, Y., Joo, Y.J., Suh, H., Batot, G., Hill, C.P., Formosa, T., and Buratowski, S. (2019). Selective Kinase Inhibition Shows That Bur1 (Cdk9) Phosphorylates the Rpb1 Linker In Vivo. Mol Cell Biol *39*.

Corden, J.L. (2013). RNA polymerase II C-terminal domain: Tethering transcription to transcript and template. Chem Rev *113*, 8423-8455.

Dion, M.F., Kaplan, T., Kim, M., Buratowski, S., Friedman, N., and Rando, O.J. (2007). Dynamics of replication-independent histone turnover in budding yeast. Science *315*, 1405-1408.

Efron, B. (1979). 1977 Rietz Lecture - Bootstrap Methods - Another Look at the Jackknife. Ann Stat *7*, 1-26.

Elf, J., and Barkefors, I. (2018). Single-Molecule Kinetics in Living Cells. Annu Rev Biochem.

Gelbart, M.E., Rechsteiner, T., Richmond, T.J., and Tsukiyama, T. (2001). Interactions of Isw2 chromatin remodeling complex with nucleosomal arrays: analyses using recombinant yeast histones and immobilized templates. Mol Cell Biol *21*, 2098-2106.

Grimaldi, Y., Ferrari, P., and Strubin, M. (2014). Independent RNA polymerase II preinitiation complex dynamics and nucleosome turnover at promoter sites in vivo. Genome Res *24*, 117-124.

Grimm, J.B., English, B.P., Chen, J., Slaughter, J.P., Zhang, Z., Revyakin, A., Patel, R., Macklin, J.J., Normanno, D., Singer, R.H.*, et al.* (2015). A general method to improve fluorophores for live-cell and single-molecule microscopy. Nat Methods *12*, 244-250, 243 p following 250.

Hansen, A.S., Woringer, M., Grimm, J.B., Lavis, L.D., Tjian, R., and Darzacq, X. (2018). Robust model-based analysis of single-particle tracking experiments with Spot-On. Elife *7*.

Harlen, K.M., and Churchman, L.S. (2017). The code and beyond: transcription regulation by the RNA polymerase II carboxy-terminal domain. Nat Rev Mol Cell Biol *18*, 263-273.

Haruki, H., Nishikawa, J., and Laemmli, U.K. (2008). The anchor-away technique: rapid, conditional establishment of yeast mutant phenotypes. Mol Cell *31*, 925-932.

Hirschhorn, J.N., Bortvin, A.L., Ricupero-Hovasse, S.L., and Winston, F. (1995). A new class of histone H2A mutations in Saccharomyces cerevisiae causes specific transcriptional defects in vivo. Mol Cell Biol *15*, 1999-2009.

Hodel, A.E., Harreman, M.T., Pulliam, K.F., Harben, M.E., Holmes, J.S., Hodel, M.R., Berland, K.M., and Corbett, A.H. (2006). Nuclear localization signal receptor affinity

correlates with in vivo localization in Saccharomyces cerevisiae. J Biol Chem *281*, 23545-23556.

Jonkers, I., and Lis, J.T. (2015). Getting up to speed with transcription elongation by RNA polymerase II. Nat Rev Mol Cell Biol *16*, 167-177.

Knoll, E.R., Zhu, Z.I., Sarkar, D., Landsman, D., and Morse, R.H. (2019). Kin28 depletion increases association of TFIID subunits Taf1 and Taf4 with promoters in Saccharomyces cerevisiae. bioRxiv.

Lai, W.K.M., and Pugh, B.F. (2017). Understanding nucleosome dynamics and their links to gene expression and DNA replication. Nat Rev Mol Cell Biol *18*, 548-562.

Lidschreiber, M., Leike, K., and Cramer, P. (2013). Cap completion and C-terminal repeat domain kinase recruitment underlie the initiation-elongation transition of RNA polymerase II. Mol Cell Biol *33*, 3805-3816.

Liu, Z., and Tjian, R. (2018). Visualizing transcription factor dynamics in living cells. J Cell Biol *217*, 1181-1191.

Lorch, Y., LaPointe, J.W., and Kornberg, R.D. (1987). Nucleosomes inhibit the initiation of transcription but allow chain elongation with the displacement of histones. Cell *49*, 203-210.

Luk, E., Ranjan, A., Fitzgerald, P.C., Mizuguchi, G., Huang, Y., Wei, D., and Wu, C. (2010). Stepwise histone replacement by SWR1 requires dual activation with histone H2A.Z and canonical nucleosome. Cell *143*, 725-736.

Luk, E., Vu, N.D., Patteson, K., Mizuguchi, G., Wu, W.H., Ranjan, A., Backus, J., Sen, S., Lewis, M., Bai, Y.*, et al.* (2007). Chz1, a nuclear chaperone for histone H2AZ. Mol Cell *25*, 357-368.

Mao, Z., Pan, L., Wang, W., Sun, J., Shan, S., Dong, Q., Liang, X., Dai, L., Ding, X., Chen, S.*, et al.* (2014). Anp32e, a higher eukaryotic histone chaperone directs preferential recognition for H2A.Z. Cell Res *24*, 389-399.

Martinez-Rucobo, F.W., Kohler, R., van de Waterbeemd, M., Heck, A.J., Hemann, M., Herzog, F., Stark, H., and Cramer, P. (2015). Molecular Basis of Transcription-Coupled Pre-mRNA Capping. Mol Cell *58*, 1079-1089.

Mizuguchi, G., Shen, X., Landry, J., Wu, W.H., Sen, S., and Wu, C. (2004). ATP-driven exchange of histone H2AZ variant catalyzed by SWR1 chromatin remodeling complex. Science *303*, 343-348.

Mohan, C., Kim, L.M., Hollar, N., Li, T., Paulissen, E., Leung, C.T., and Luk, E. (2018). VivosX, a disulfide crosslinking method to capture site-specific, protein-protein interactions in yeast and human cells. Elife *7*.

Morillo-Huesca, M., Clemente-Ruiz, M., Andujar, E., and Prado, F. (2010). The SWR1 histone replacement complex causes genetic instability and genome-wide transcription misregulation in the absence of H2A.Z. PLoS One *5*, e12143.

Murakami, K., Mattei, P.J., Davis, R.E., Jin, H., Kaplan, C.D., and Kornberg, R.D. (2015). Uncoupling Promoter Opening from Start-Site Scanning. Mol Cell *59*, 133-138.

Obri, A., Ouararhni, K., Papin, C., Diebold, M.L., Padmanabhan, K., Marek, M., Stoll, I., Roy, L., Reilly, P.T., Mak, T.W.*, et al.* (2014). ANP32E is a histone chaperone that removes H2A.Z from chromatin. Nature *505*, 648-653.

Papamichos-Chronakis, M., Watanabe, S., Rando, O.J., and Peterson, C.L. (2011). Global regulation of H2A.Z localization by the INO80 chromatin-remodeling enzyme is essential for genome integrity. Cell *144*, 200-213.

Pelechano, V., Wei, W., and Steinmetz, L.M. (2013). Extensive transcriptional heterogeneity revealed by isoform profiling. Nature *497*, 127-131.

Qian, H., Sheetz, M.P., and Elson, E.L. (1991). Single particle tracking. Analysis of diffusion and flow in two-dimensional systems. Biophys J *60*, 910-921.

Ranjan, A., Mizuguchi, G., FitzGerald, P.C., Wei, D., Wang, F., Huang, Y., Luk, E., Woodcock, C.L., and Wu, C. (2013). Nucleosome-free region dominates histone acetylation in targeting SWR1 to promoters for H2A.Z replacement. Cell *154*, 1232-1245.

Rhee, H.S., and Pugh, B.F. (2012). Genome-wide structure and organization of eukaryotic pre-initiation complexes. Nature *483*, 295-301.

Rufiange, A., Jacques, P.E., Bhat, W., Robert, F., and Nourani, A. (2007). Genome-wide replication-independent histone H3 exchange occurs predominantly at promoters and implicates H3 K56 acetylation and Asf1. Mol Cell *27*, 393-405.

Rust, M.J., Bates, M., and Zhuang, X. (2006). Sub-diffraction-limit imaging by stochastic optical reconstruction microscopy (STORM). Nat Methods *3*, 793-795.

Sainsbury, S., Bernecky, C., and Cramer, P. (2015). Structural basis of transcription initiation by RNA polymerase II. Nat Rev Mol Cell Biol *16*, 129-143.

Schaughency, P., Merran, J., and Corden, J.L. (2014). Genome-Wide Mapping of Yeast RNA Polymerase II Termination. Plos Genetics *10*.

Shim, S.H., Xia, C., Zhong, G., Babcock, H.P., Vaughan, J.C., Huang, B., Wang, X., Xu, C., Bi, G.Q., and Zhuang, X. (2012). Super-resolution fluorescence imaging of organelles in live cells with photoswitchable membrane probes. Proc Natl Acad Sci U S A *109*, 13978-13983.

Sun, L., and Luk, E. (2017). Dual function of Swc5 in SWR remodeling ATPase activation and histone H2A eviction. Nucleic Acids Res *45*, 9931-9946.

Taddei, A., and Gasser, S.M. (2012). Structure and function in the budding yeast nucleus. Genetics *192*, 107-129.

Tippens, N.D., Vihervaara, A., and Lis, J.T. (2018). Enhancer transcription: what, where, when, and why? Genes Dev *32*, 1-3.

Tome, J.M., Tippens, N.D., and Lis, J.T. (2018). Single-molecule nascent RNA sequencing identifies regulatory domain architecture at promoters and enhancers. Nat Genet *50*, 1533-1541.

Tramantano, M., Sun, L., Au, C., Labuz, D., Liu, Z., Chou, M., Shen, C., and Luk, E. (2016). Constitutive turnover of histone H2A.Z at yeast promoters requires the preinitiation complex. Elife *5*.

Vallotton, P., and Olivier, S. (2013). Tri-track: free software for large-scale particle tracking. Microsc Microanal *19*, 451-460.

Wang, F., Ranjan, A., Wei, D., and Wu, C. (2016). Comment on "A histone acetylation switch regulates H2A.Z deposition by the SWR-C remodeling enzyme". Science *353*, 358.

Watanabe, S., Radman-Livaja, M., Rando, O.J., and Peterson, C.L. (2013). A histone acetylation switch regulates H2A.Z deposition by the SWR-C remodeling enzyme. Science *340*, 195-199.

Weber, C.M., and Henikoff, S. (2014). Histone variants: dynamic punctuation in transcription. Genes Dev *28*, 672-682.

Wong, K.H., Jin, Y., and Struhl, K. (2014). TFIIH phosphorylation of the Pol II CTD stimulates mediator dissociation from the preinitiation complex and promoter escape. Mol Cell *54*, 601-612.

Yen, K., Vinayachandran, V., and Pugh, B.F. (2013). SWR-C and INO80 chromatin remodelers recognize nucleosome-free regions near +1 nucleosomes. Cell *154*, 1246-1256.

Zheng, Q., Ayala, A.X., Chung, I., Weigel, A.V., Ranjan, A., Falco, N., Grimm, J.B., Tkachuk, A.N., Wu, C., Lippincott-Schwartz, J.*, et al.* (2019). Rational Design of Fluorogenic and Spontaneously Blinking Labels for Super-Resolution Imaging. ACS Cent Sci *5*, 1602-1613.

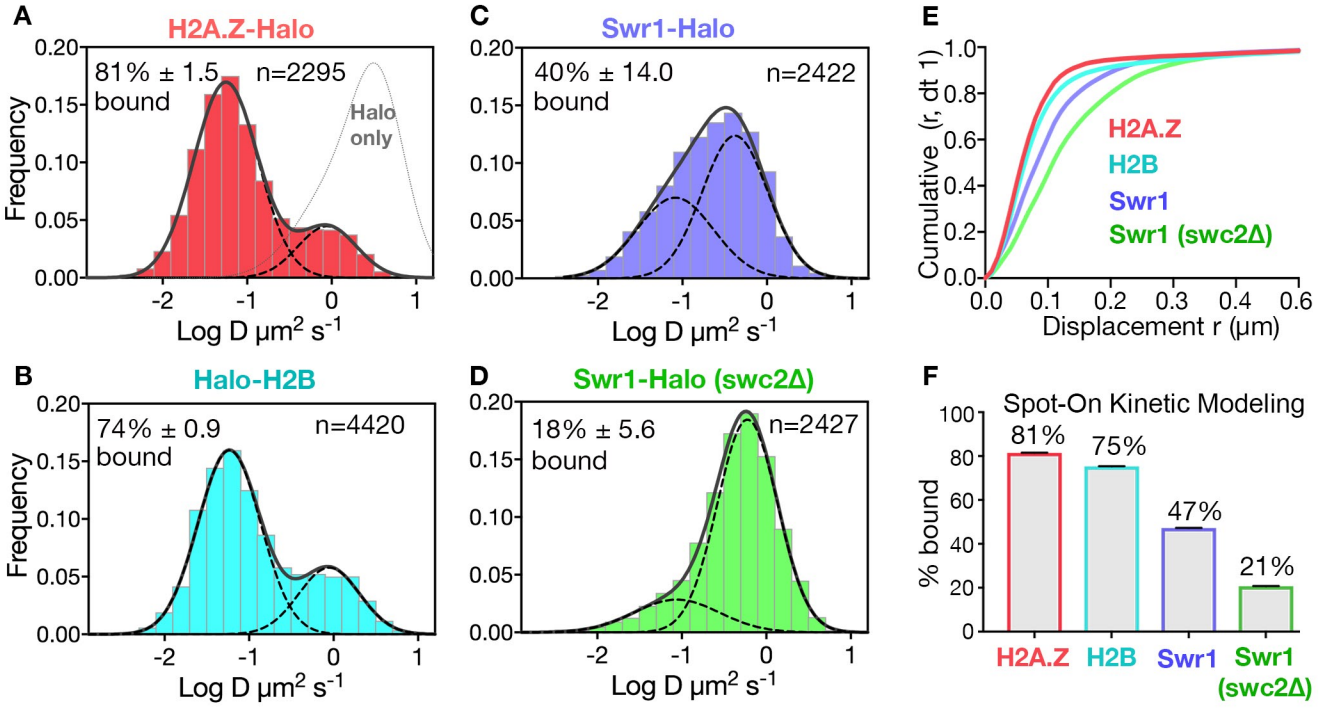
A
H2A.Z-Halo
81% ± 1.5 bound
n=2295
Halo only
Frequency
Log D µm² s⁻¹
B
Halo-H2B
74% ± 0.9 bound
n=4420
C
Swr1-Halo
40% ± 14.0 bound
n=2422
D
Swr1-Halo (swc2Δ)
18% ± 5.6 bound
n=2427
E
Cumulative (r, dt 1)
Displacement r (µm)
H2A.Z
H2B
Swr1
Swr1 (swc2Δ)
F
Spot-On Kinetic Modeling
% bound
81%
75%
47%
21%
H2A.Z
H2B
Swr1
Swr1 (swc2Δ)

Fig. 1

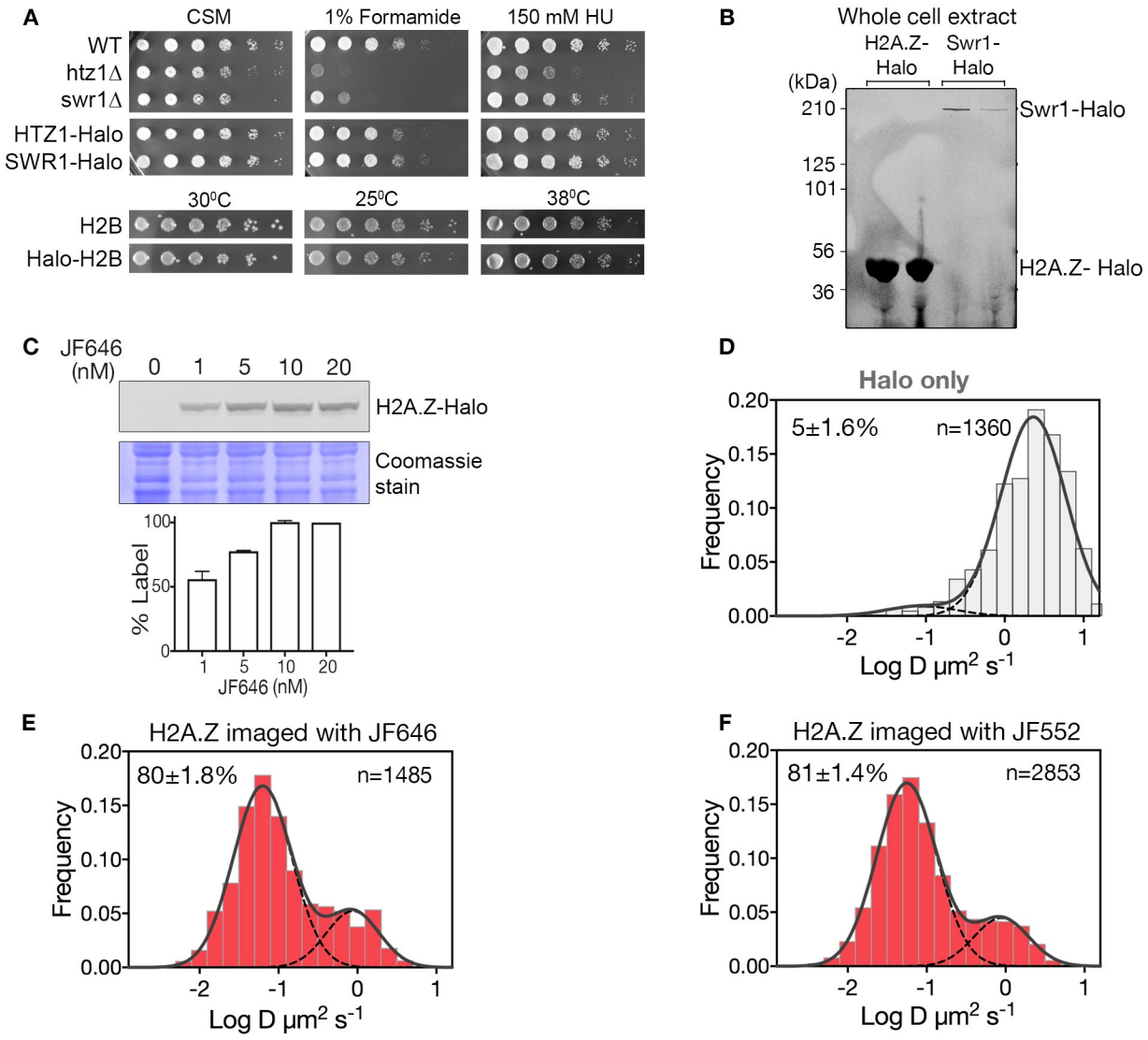
A
CSM
1% Formamide
150 mM HU
WT
htz1Δ
swr1Δ
HTZ1-Halo
SWR1-Halo
30⁰C
25⁰C
38⁰C
H2B
Halo-H2B
B
Whole cell extract
H2A.Z-Halo
Swr1-Halo
(kDa)
210
125
101
56
36
Swr1-Halo
H2A.Z- Halo
C
JF646 (nM)
0 1 5 10 20
H2A.Z-Halo
Coomassie stain
% Label
100
50
0
1 5 10 20
JF646 (nM)
D
Halo only
5±1.6%
n=1360
Frequency
0.20
0.15
0.10
0.05
0.00
-2 -1 0 1
Log D μm² s⁻¹
E
H2A.Z imaged with JF646
80±1.8%
n=1485
Frequency
Log D μm² s⁻¹
F
H2A.Z imaged with JF552
81±1.4%
n=2853
Frequency
Log D μm² s⁻¹

Fig. S1.1

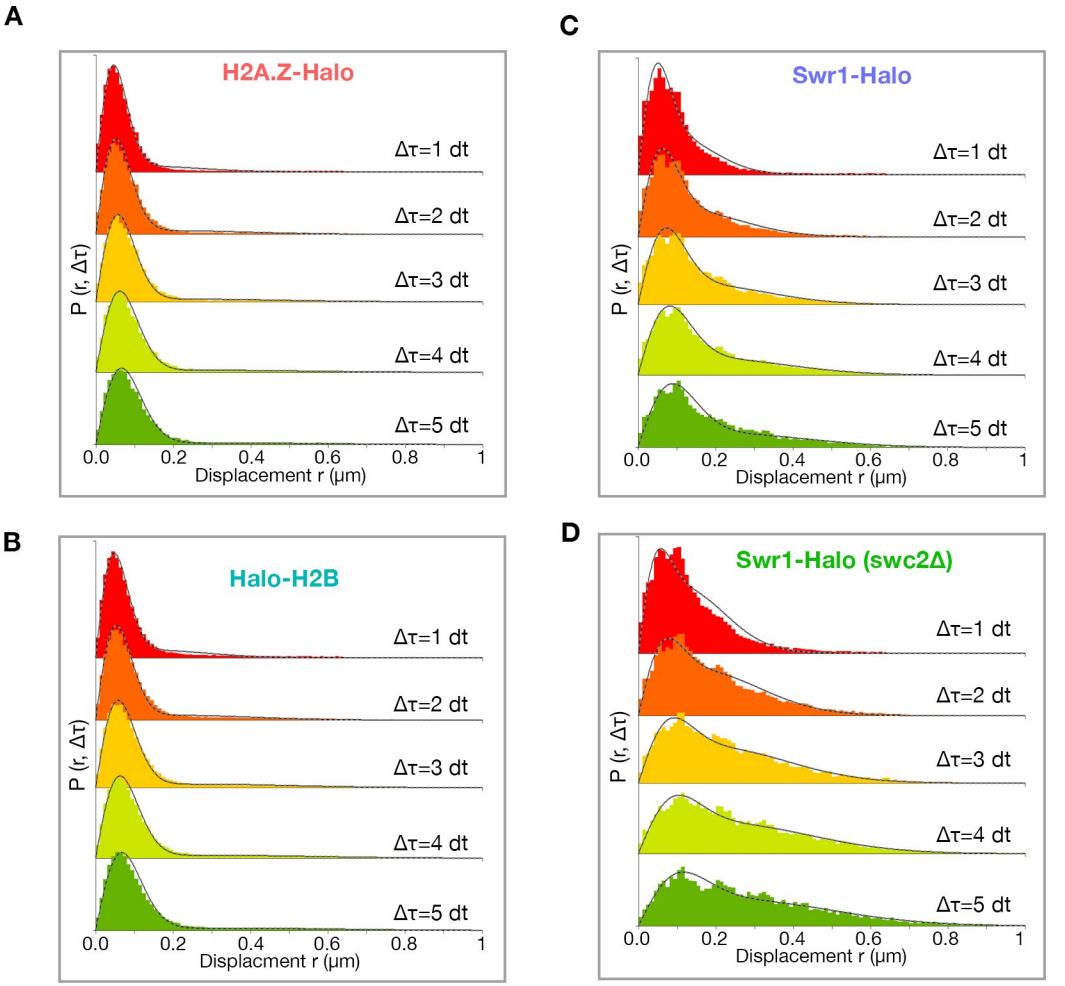

E

	MSD			Spot-On		
	D bound ($\mu m^2\ s^{-1}$)	D free ($\mu m^2\ s^{-1}$)	% bound	D bound ($\mu m^2\ s^{-1}$)	D free ($\mu m^2\ s^{-1}$)	% bound
H2A.Z	0.056 ± 0.002	0.886 ± 0.066	80.5 ± 1.54	0.029 ± 0.0002	1.177 ± 0.009	81.7 ± 0.07
H2B	0.058 ± 0.001	0.888 ± 0.039	73.9 ± 0.99	0.028 ± 0.0002	1.286 ± 0.008	75.6 ± 0.06
Swr1	0.082 ± 0.028	0.419 ± 0.066	39.7 ± 14.07	0.063 ± 0.0003	0.618 ± 0.002	47.2 ± 0.11
Swr1 (swc2Δ)	0.087 ± 0.034	0.598 ± 0.026	18.0 ± 5.64	0.070 ± 0.0001	0.766 ± 0.001	20.7 ± 0.07

Fig. S1.2

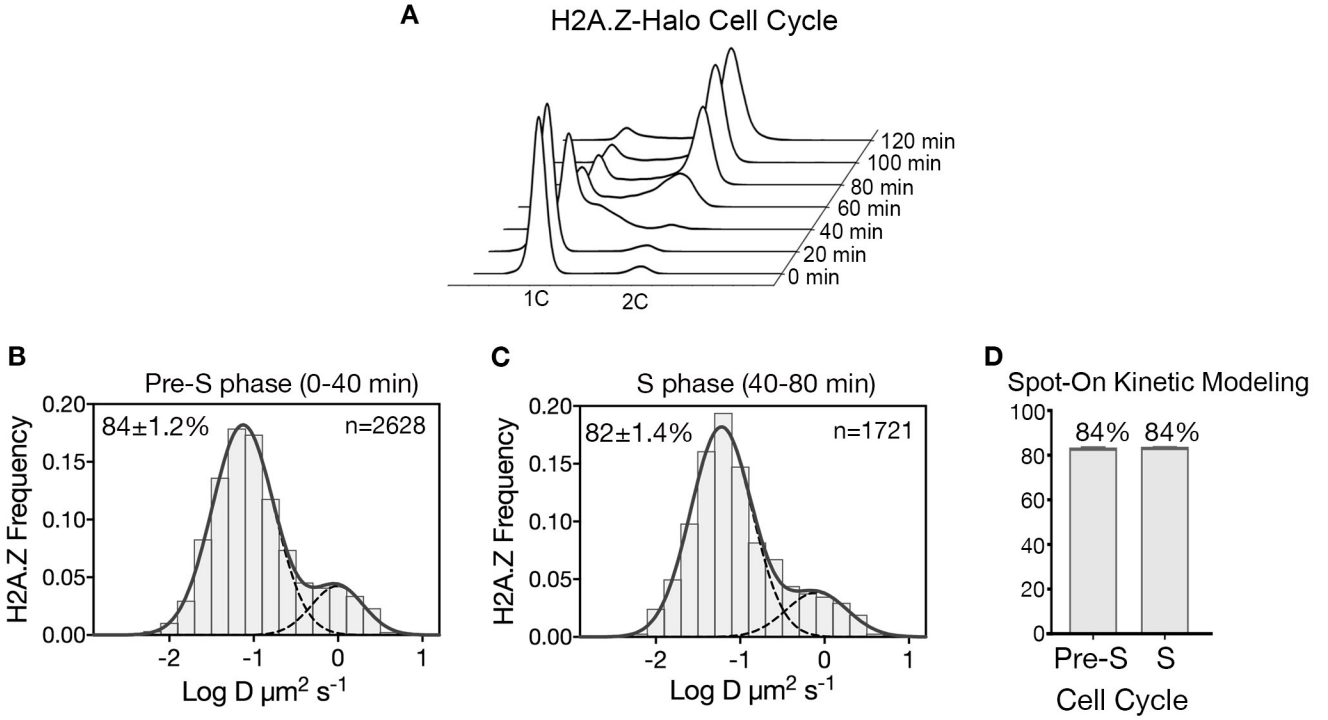
A
H2A.Z-Halo Cell Cycle
120 min
100 min
80 min
60 min
40 min
20 min
0 min
1C
2C
B
Pre-S phase (0-40 min)
84±1.2%
n=2628
H2A.Z Frequency
Log D µm² s⁻¹
C
S phase (40-80 min)
82±1.4%
n=1721
H2A.Z Frequency
Log D µm² s⁻¹
D
Spot-On Kinetic Modeling
84% 84%
Pre-S S
Cell Cycle

Fig. S1.3

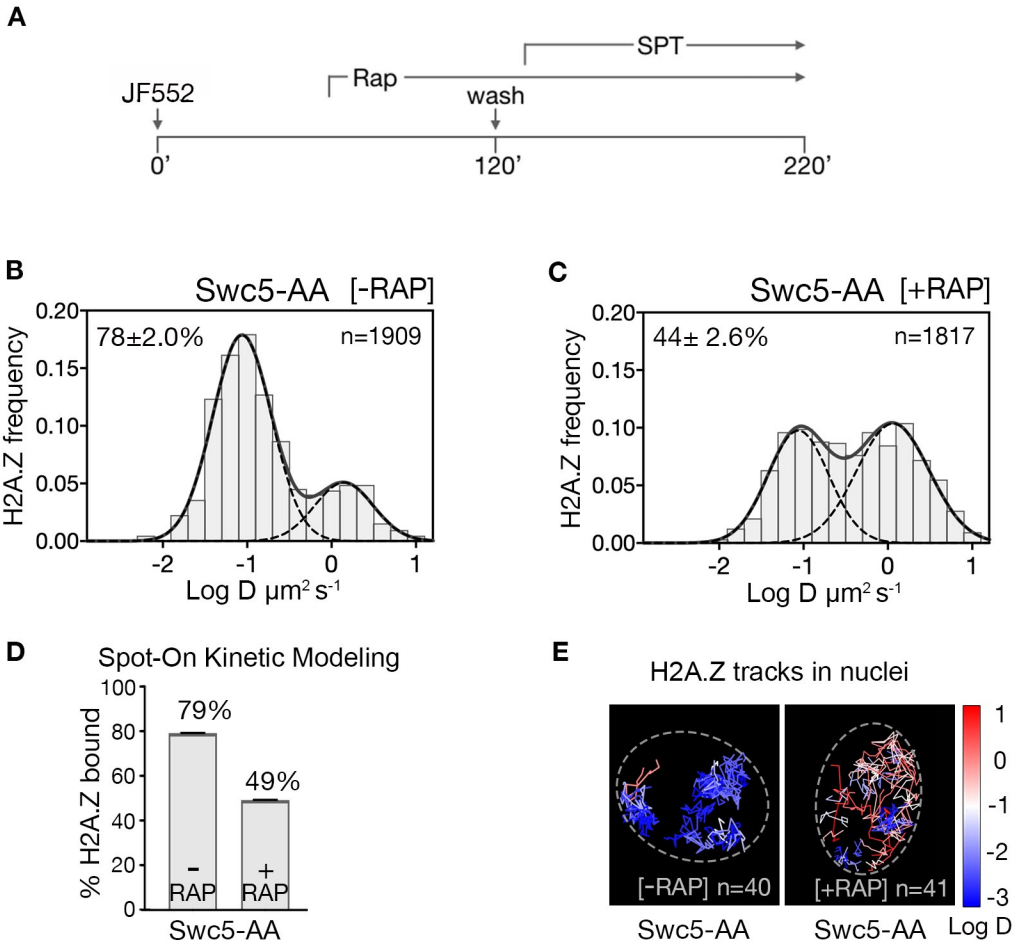
A
SPT
Rap
JF552
wash
0'
120'
220'
B
Swc5-AA [-RAP]
78±2.0%
n=1909
H2A.Z frequency
Log D µm² s⁻¹
C
Swc5-AA [+RAP]
44± 2.6%
n=1817
H2A.Z frequency
Log D µm² s⁻¹
D
Spot-On Kinetic Modeling
% H2A.Z bound
79%
49%
- RAP
+ RAP
Swc5-AA
E
H2A.Z tracks in nuclei
[-RAP] n=40
[+RAP] n=41
Swc5-AA
Swc5-AA
Log D

Fig. 2

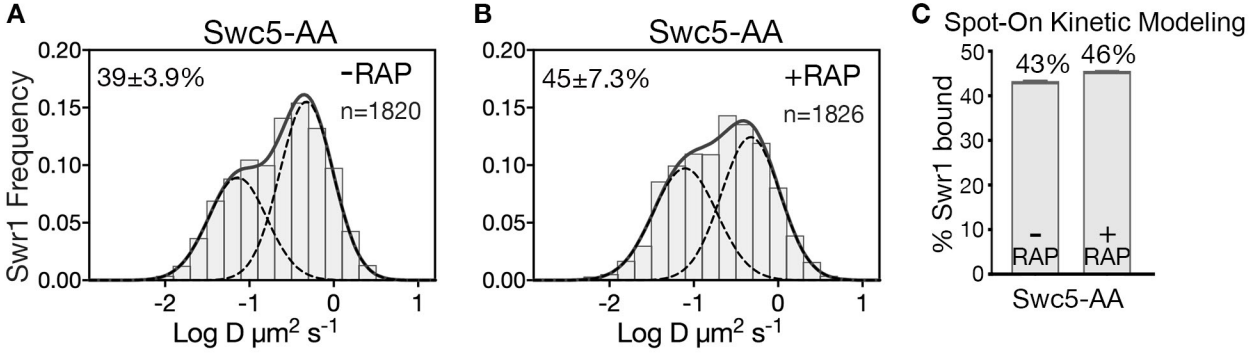
A
Swc5-AA
39±3.9%
-RAP
n=1820
Swr1 Frequency
0.20
0.15
0.10
0.05
0.00
-2
-1
0
1
Log D μm² s⁻¹
B
Swc5-AA
45±7.3%
+RAP
n=1826
Log D μm² s⁻¹
C
Spot-On Kinetic Modeling
% Swr1 bound
50
40
30
20
10
0
43%
46%
-
RAP
+
RAP
Swc5-AA

Fig. S2.1

Double AA conditions below to be compared with Fig. 2C,D

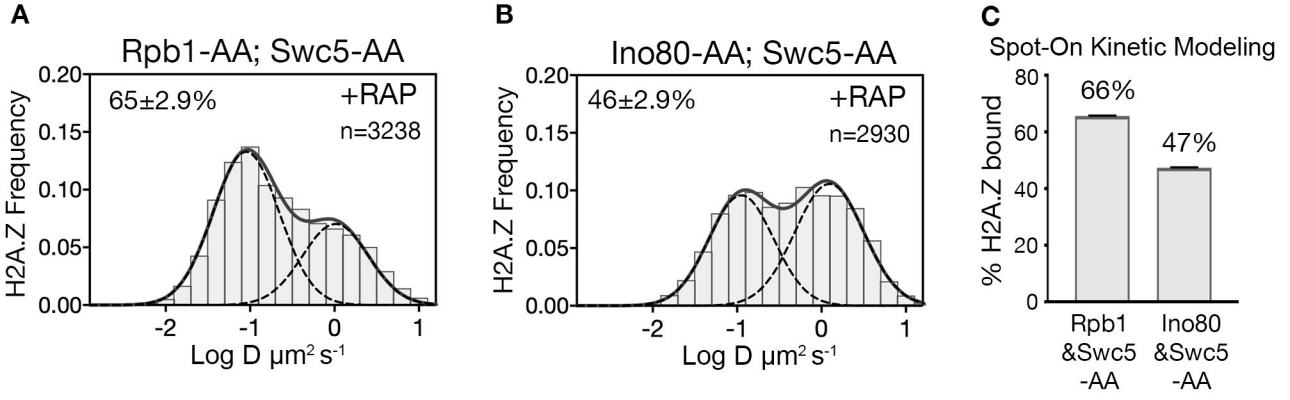

Fig. 3

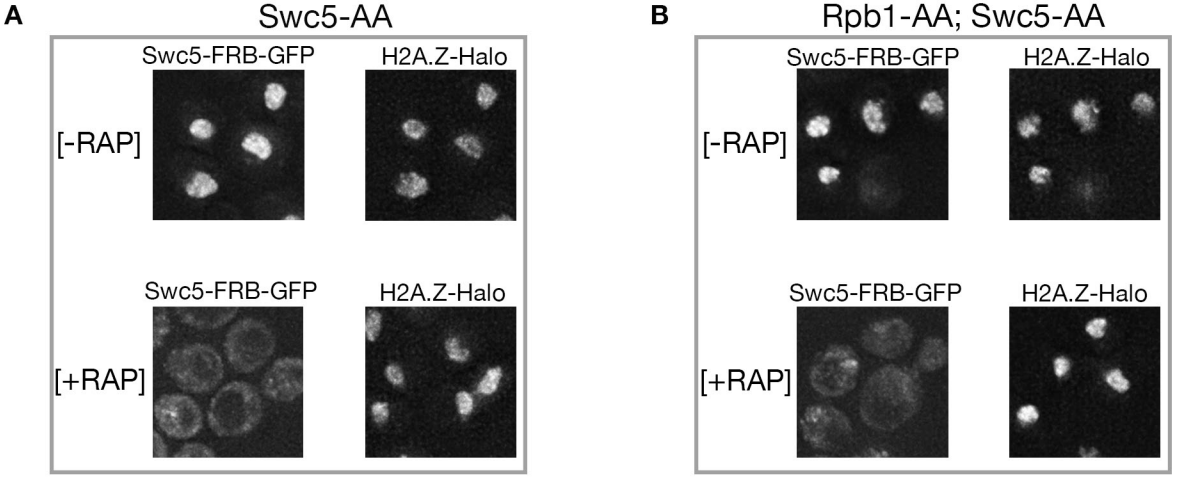
A
Swc5-AA
Swc5-FRB-GFP
H2A.Z-Halo
[-RAP]
Swc5-FRB-GFP
H2A.Z-Halo
[+RAP]
B
Rpb1-AA; Swc5-AA
Swc5-FRB-GFP
H2A.Z-Halo
[-RAP]
Swc5-FRB-GFP
H2A.Z-Halo
[+RAP]

Fig. S3.1

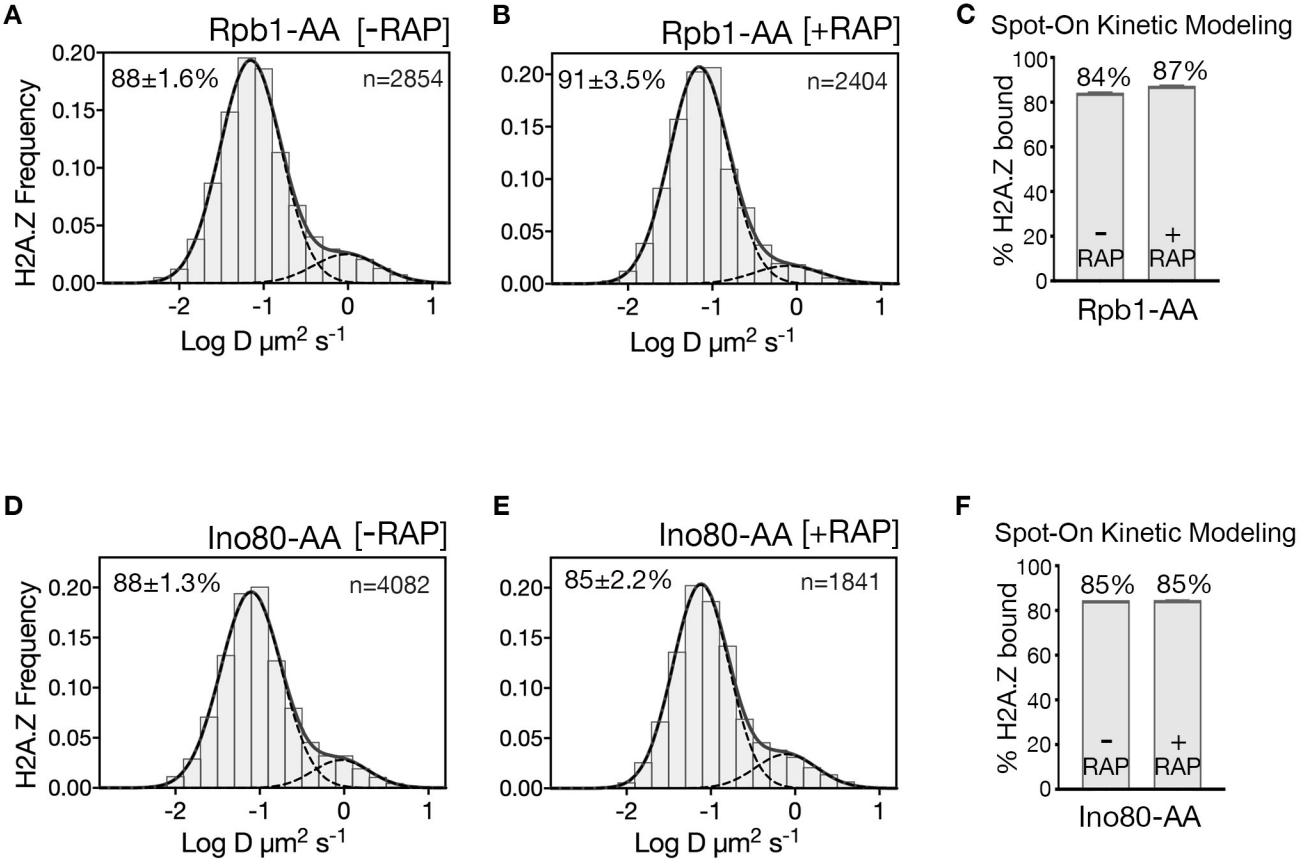
A
Rpb1-AA [-RAP]
88±1.6%
n=2854
H2A.Z Frequency
Log D μm² s⁻¹
B
Rpb1-AA [+RAP]
91±3.5%
n=2404
Log D μm² s⁻¹
C
Spot-On Kinetic Modeling
% H2A.Z bound
84%
87%
- RAP
+ RAP
Rpb1-AA
D
Ino80-AA [-RAP]
88±1.3%
n=4082
H2A.Z Frequency
Log D μm² s⁻¹
E
Ino80-AA [+RAP]
85±2.2%
n=1841
Log D μm² s⁻¹
F
Spot-On Kinetic Modeling
% H2A.Z bound
85%
85%
- RAP
+ RAP
Ino80-AA

Fig. S3.2

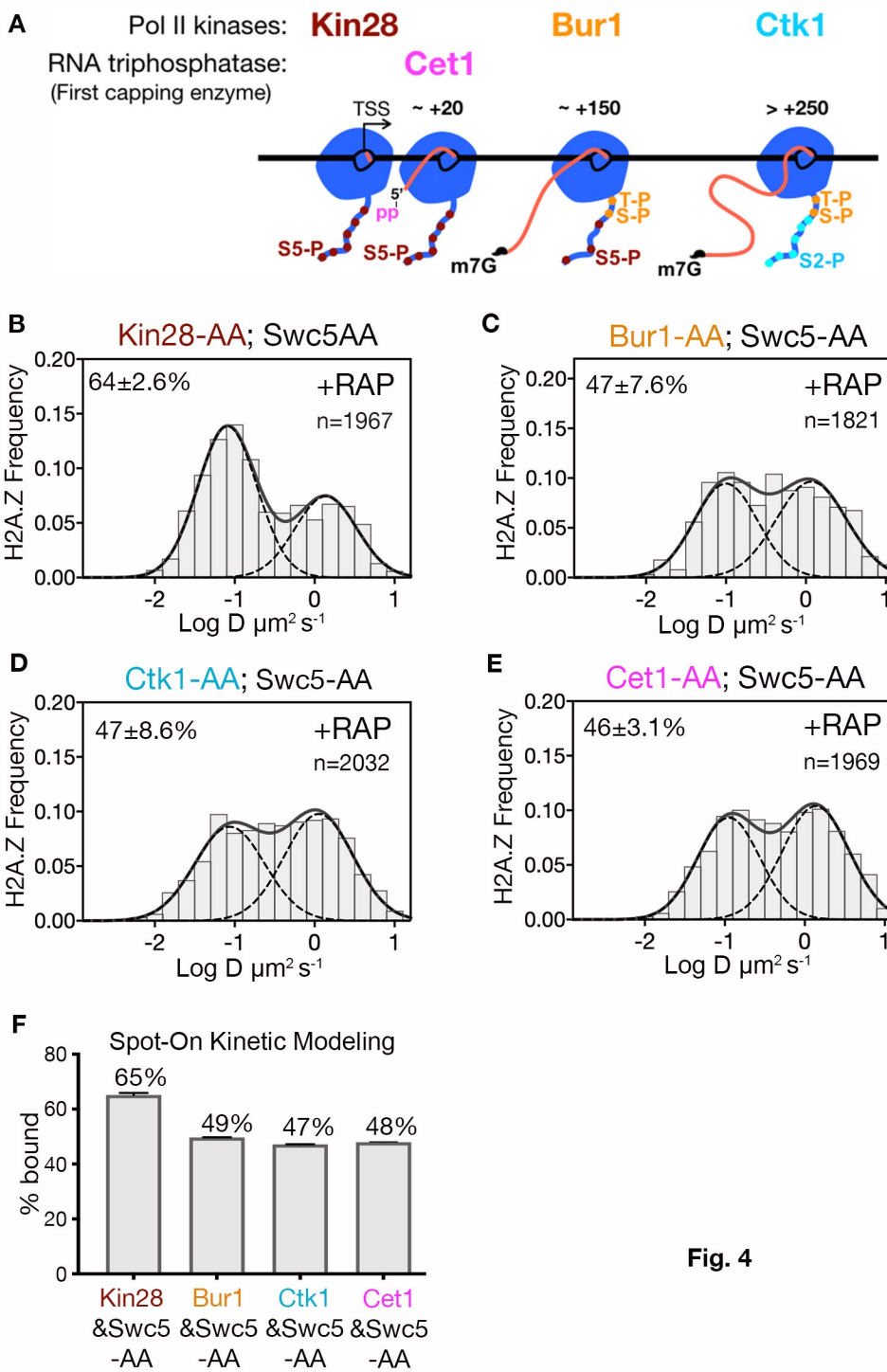
A
Pol II kinases: Kin28 Bur1 Ctk1
RNA triphosphatase: Cet1
(First capping enzyme)
TSS
~ +20
~ +150
> +250
5'
pp
S5-P
S5-P
m7G
S5-P
T-P
S-P
m7G
S2-P
T-P
S-P
B
Kin28-AA; Swc5AA
64±2.6%
+RAP
n=1967
C
Bur1-AA; Swc5-AA
47±7.6%
+RAP
n=1821
D
Ctk1-AA; Swc5-AA
47±8.6%
+RAP
n=2032
E
Cet1-AA; Swc5-AA
46±3.1%
+RAP
n=1969
H2A.Z Frequency
Log D μm² s⁻¹
F
Spot-On Kinetic Modeling
% bound
65%
49%
47%
48%
Kin28 &Swc5 -AA
Bur1 &Swc5 -AA
Ctk1 &Swc5 -AA
Cet1 &Swc5 -AA

Fig. 4

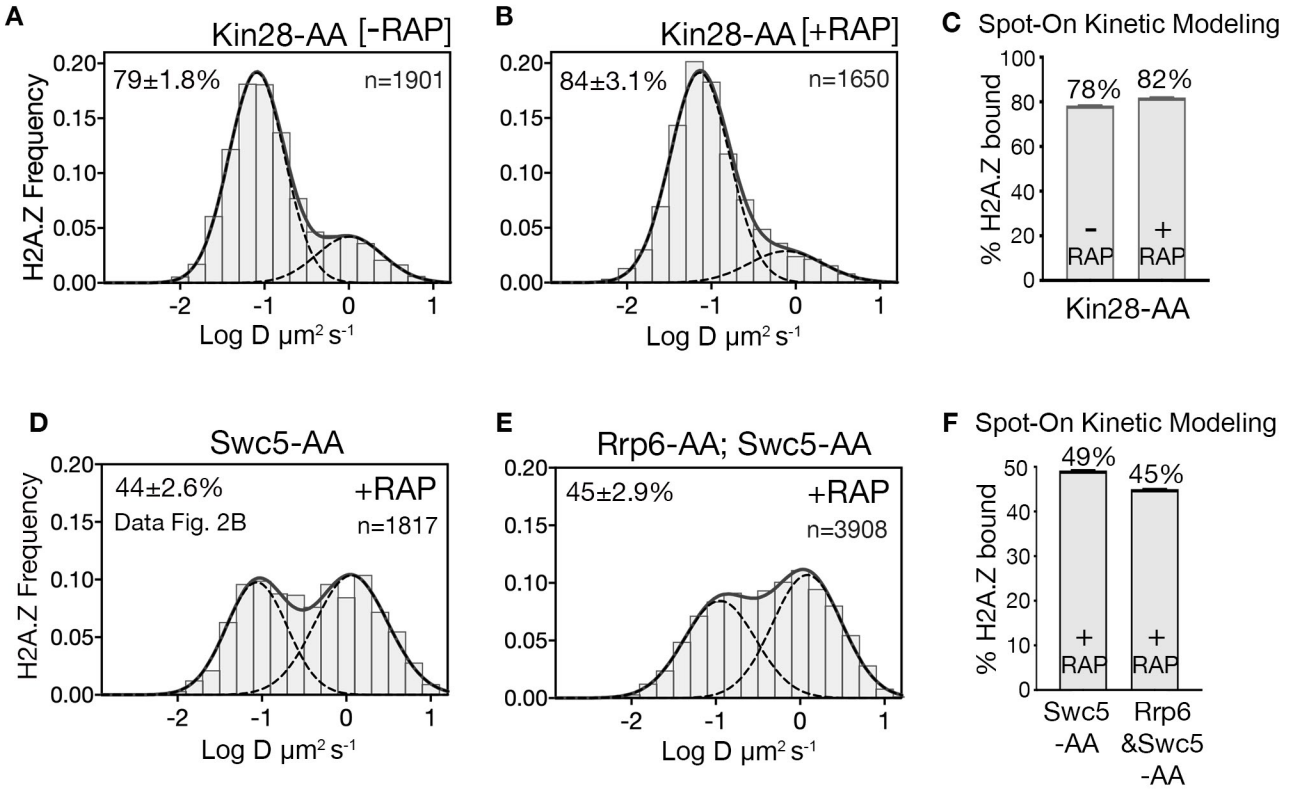
A
Kin28-AA [-RAP]
79±1.8%
n=1901
H2A.Z Frequency
Log D μm² s⁻¹
B
Kin28-AA [+RAP]
84±3.1%
n=1650
C
Spot-On Kinetic Modeling
% H2A.Z bound
78%
82%
- RAP
+ RAP
Kin28-AA
D
Swc5-AA
44±2.6%
Data Fig. 2B
+RAP
n=1817
E
Rrp6-AA; Swc5-AA
45±2.9%
+RAP
n=3908
F
Spot-On Kinetic Modeling
49%
45%
Swc5 -AA
Rrp6 &Swc5 -AA

Fig. S4.1

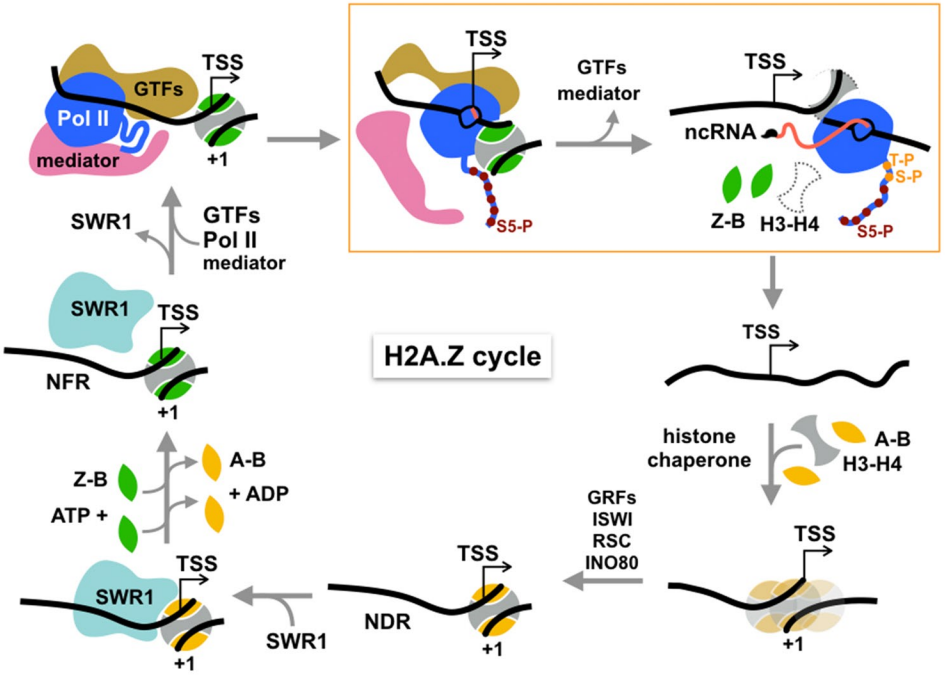
TSS
GTFs
Pol II
mediator
+1
GTFs
mediator
TSS
ncRNA
T-P
S-P
Z-B
H3-H4
S5-P
S5-P
TSS
histone
chaperone
A-B
H3-H4
GRFs
ISWI
RSC
INO80
TSS
+1
TSS
NDR
+1
SWR1
TSS
SWR1
+1
Z-B
ATP +
A-B
+ ADP
SWR1
GTFs
Pol II
mediator
SWR1
TSS
NFR
+1
H2A.Z cycle

Fig. 5